Electronic Supplementary Material (ESI) for Energy & Environmental Science.
This journal is © The Royal Society of Chemistry 2022

High performance dual-electrolyte based magnesium-iodine batteries that can harmlessly resorb in the environment or in the body

Ivy Huang[1,2,3†], Yamin Zhang[1,2†], Hany M. Arafa[1,2,4], Shupeng Li[5], Abraham Vazquez-Guardado[1,2], Wei Ouyang[1,2], Fei Liu[1,2,3], Surabhi Madhvapathy[1,2,3], Joseph Woojin Song[4], Andreas Tzavelis[1,2,4], Jacob Trueb[1,2], Yeonsik Choi[1,2], William J. Jeang[1,2], Viviane Forsberg[1,2,6], Elizabeth Dempsey[7], Nayereh Ghoreishi-Haack[7], Iwona Stepien[7], Keith Bailey[9], Shuling Han[9,10], Zheng Jenny Zhang[9,10], Cameron Good[1,2], Yonggang Huang[2,3,4,11], Amay J. Bandodkar[12]*, John A. Rogers[1,2,3,4,5,13]*

[1]Center for Bio-Integrated Electronics, Northwestern University, Evanston, IL, USA.

[2]Querrey Simpson Institute for Bioelectronics, Northwestern University, Evanston, IL, USA.

[3]Department of Materials Science and Engineering, Northwestern University, Evanston, IL, USA.

[4]Department of Biomedical Engineering, Northwestern University, Evanston, IL, USA.

[5]Department of Mechanical Engineering, Northwestern University, Evanston, IL, USA.

[6]Department of Natural Sciences, Mid Sweden University, Holmgatan, Sundsvall, Sweden.

[7]Developmental Therapeutics Core, Northwestern University, Evanston, IL, USA.

[8]Charles River Laboratories, Mattawan, MI, USA.

[9]Comprehensive Transplant Center, Feinberg School of Medicine, Northwestern University, Chicago, IL, USA.

[10]Department of Surgery, Feinberg School of Medicine, Northwestern University, Chicago, IL, USA.

[11]Department of Civil and Environmental Engineering, Northwestern University, Evanston, IL, USA.

[12]Department of Electrical and Computer Engineering, North Carolina State University, Raleigh, NC, USA.

[13]Department of Neurological Surgery, Feinberg School of Medicine, Northwestern University, Chicago, IL, USA.

†These authors contributed equally.

*Correspondence: jrogers@northwestern.edu and ajbandod@ncsu.edu

High voltage output (> 1.8 V) and large cell capacity (~ 2.45 mAh) with small cell size (~ 0.5 cm length * 0.5 cm width * 0.19 cm height) are achieved. The calculations are listed below.

$$\text{Areal capacity } (mAh\ cm^{-2}) = \frac{Capacity}{Area} = \frac{2.45}{0.5 * 0.5} = 9.8$$

$$\text{Areal energy } (mWh\ cm^{-2}) = \frac{Capacity * Voltage}{Area} = \frac{2.45 * 1.8}{0.5 * 0.5} = 17.7$$

$$\text{Volumetric energy } (mWh\ cm^{-3}) = \frac{Capacity * Voltage}{Volume} = \frac{2.45 * 1.8}{0.5 * 0.5 * 0.19} = 93$$

$$\text{Areal power } (mW\ cm^{-2}) = \frac{Current * Voltage}{Area} = \frac{0.4 * 1.8}{0.5 * 0.5} = 0.72$$

$$\text{Volumetric power } (mW\ cm^{-3}) = \frac{Current * Voltage}{Volume} = \frac{0.4 * 1.8}{0.5 * 0.5 * 0.19} = 3.8$$

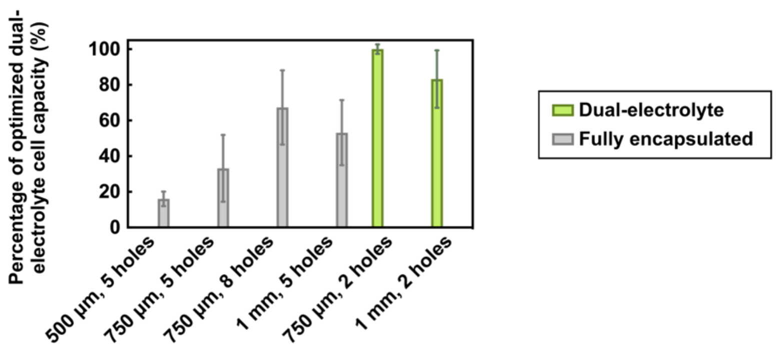

Supplementary Figure 1. Optimization of the polyanhydride encapsulation structure. Results correspond to configurations with different numbers and sizes of holes for *(green)* dual-electrolyte and *(grey)* fully encapsulated cell architectures. In the latter, both the cathode and anode are encapsulated. The areal capacity of each group corresponds to the percentage of the value obtained with the optimized cell configuration. n=3 cells per group.

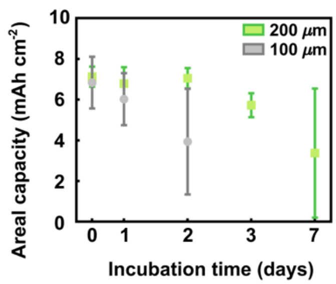

Supplementary Figure 2. Effect of incubation time in PBS on areal capacity for cells with 100 µm and 200 µm thick Mg anodes and 300 µm Ag/AgCl cathodes. Cells are immersed in chicken breast and PBS (pH 7.4) at 37 °C for 0, 1, 2, 3, and 7 days. n=3 cells per day. Setting: 4 mA cm^{-2}.

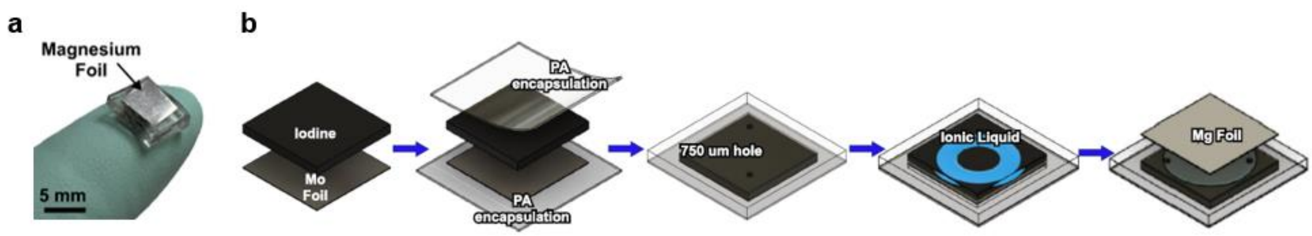

Supplementary Figure 3. Characteristics of the battery. a, Optical image of a cell vertically stacked. **b,** Fabrication schematic of the Mg/I_2 cell.

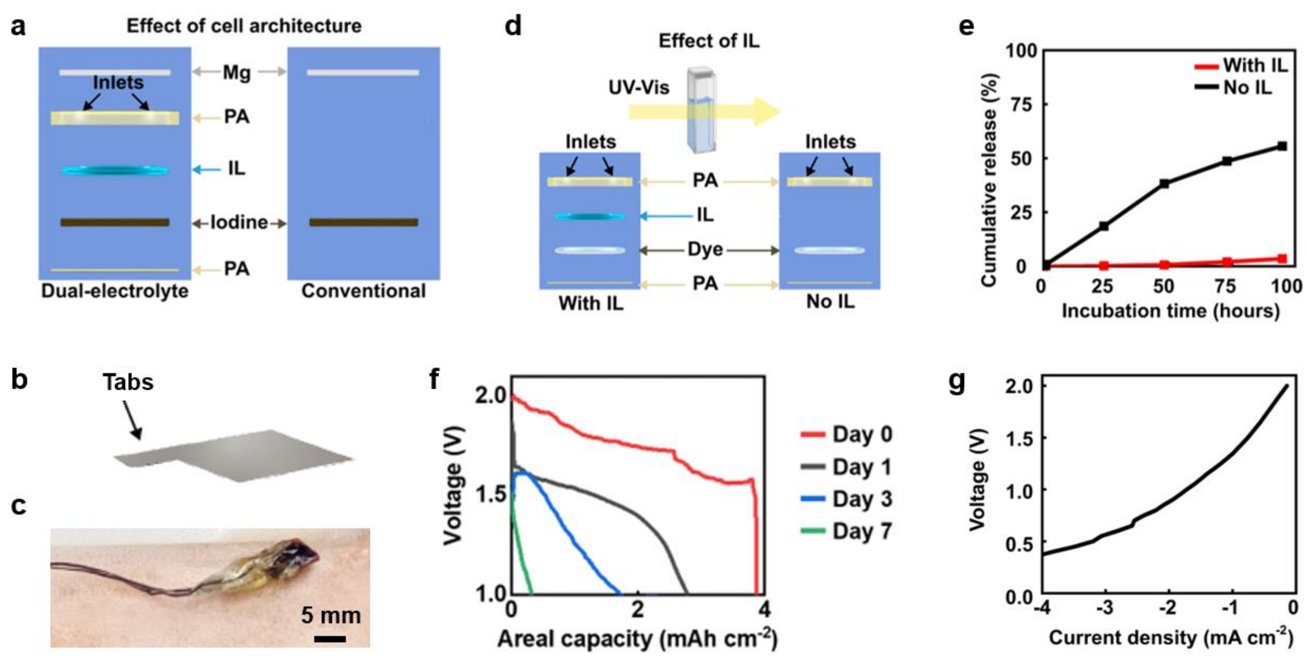

Supplementary Figure 4. **a**, Effect of cell architecture on performance. Cross-sectional schematic illustration of cells assembled with *(left)* dual-electrolyte and a *(Right)* conventional configuration. The dual-electrolyte cell architecture features an encapsulated iodine cathode surrounded by ionic liquid. The conventional version does not feature encapsulation or ionic liquid. **b**, LPKF cutting design of electrode current collector. **c**, Optical image of a cell with conductive wires. **d**, Effect of ionic liquid in a dual-electrolyte assembly observed through the cumulative release of a dye over time. The dye represents the iodine cathode. *(Left)* Cross-sectional schematic illustration of dye and ionic liquid and *(right)* only dye, without ionic liquid. **e**, **C**umulative release of a dye over time**.** **f**, Plots of discharge behaviors of the Mg/I_2 cell after immersion in PBS (pH 7.4) at 37 °C. **g**, Linear sweep voltammetry (LSV) curves for the eco/bioresorbable cell in PBS. n=3 cells.

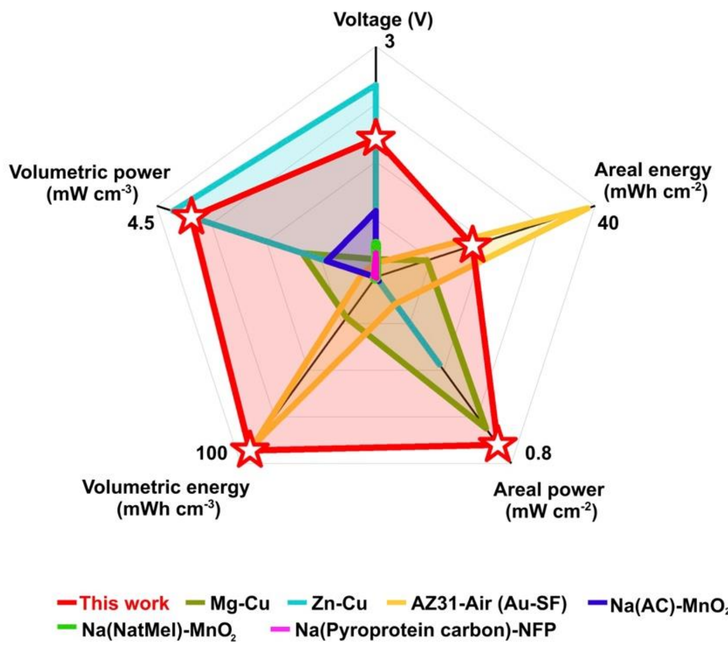

Supplementary Figure 5. Radar plot comparison of performance characteristics of the battery technology reported here and other non-bioresorbable, implantable cells (Mg-Cu[1], Zn-Cu[1], AZ31-Air (Au-SF)[2], Na(AC)-MnO_2[3], Na(NatMel)-MnO_2[4], Na(Pyroprotein carbon)-NFP[5]).

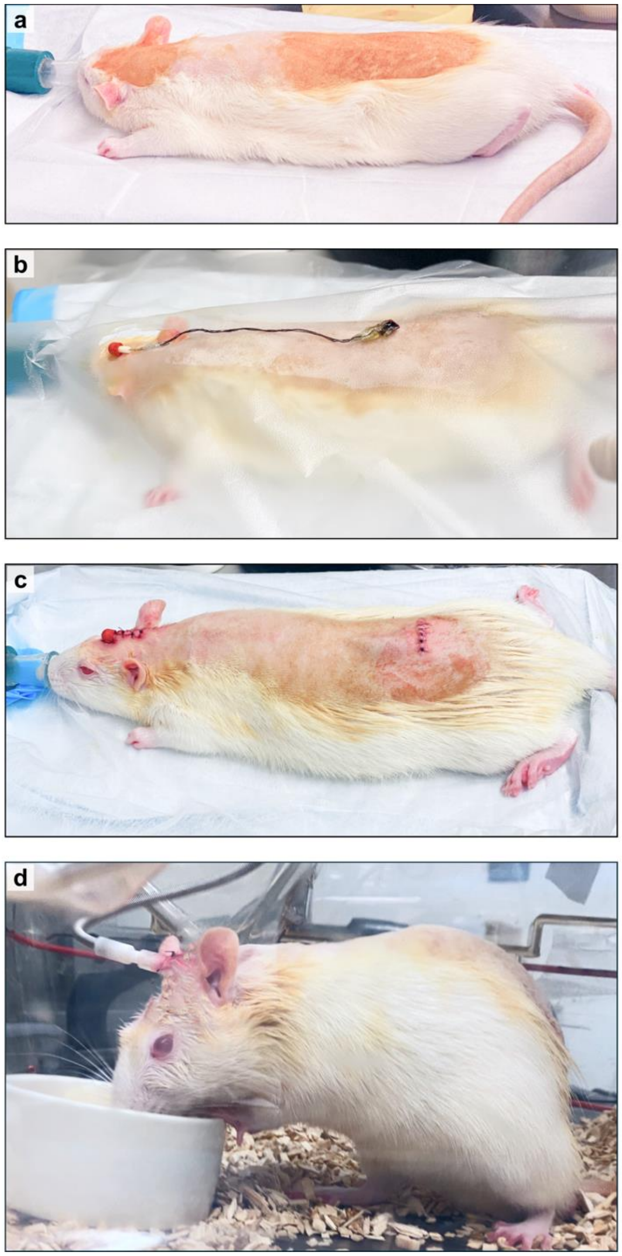

Supplementary Figure 6. Surgical preparations for *in vivo* studies of the capacities of implanted cells. Surgical procedure for implanting a cell inside a small animal (rat) model. **a,** Rat shaved at the target site and cleaned with iodine. **b,** Location for implantation is identified and the cell, wires, and headcap are approximately positioned. A tunnel along the fascial tissue from the head to the back forms a route for wires that tunnel from head to back. **c,** Sutures are applied along the head and back to finish the procedure. **d,** Image of rat post-surgical procedure.

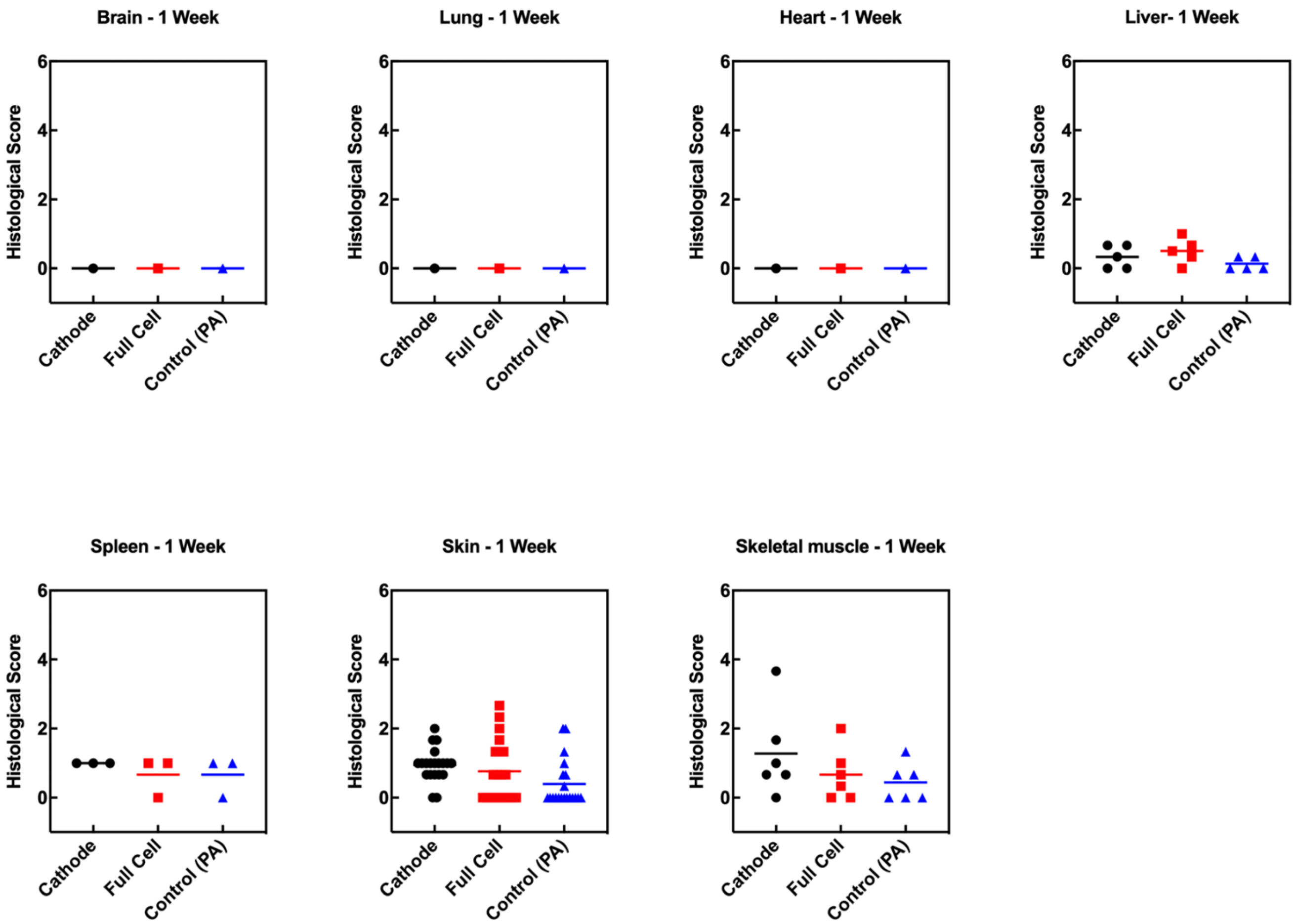

Supplementary Figure 7. 5 grade scoring system after 1 week of implantation. Severity Score: 0 = finding not observed, 1 = minimal, 2 = mild, 3 = moderate, 4 = marked, 5 = severe. Distribution modifier: D = diffuse, F = focal, M = multifocal. P = non-gradable finding is present, NP = tissue/slide not present, NA = not available. Microscopic findings identified in control animals are common spontaneous observations that occur in toxicologic pathology studies.

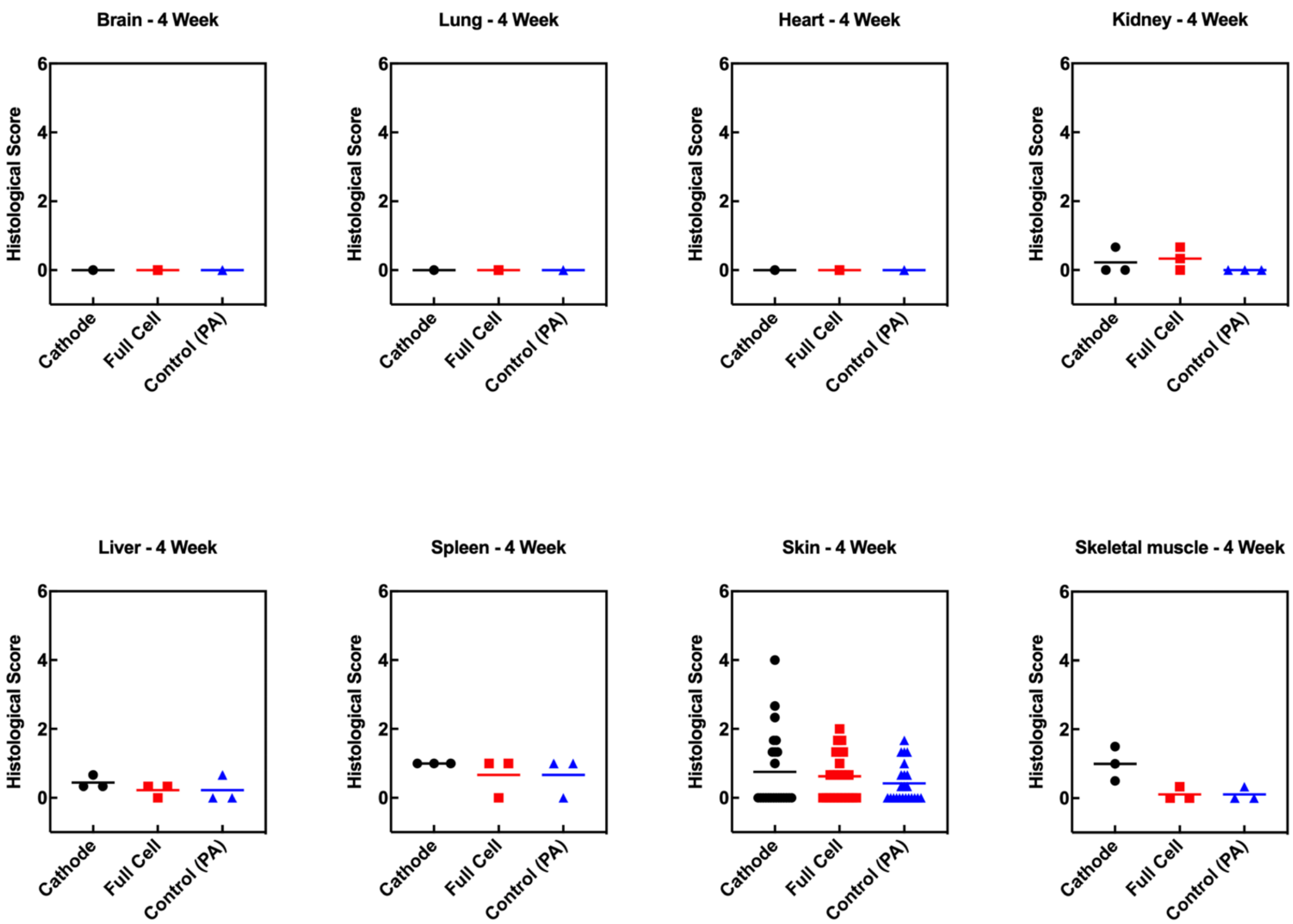

Supplementary Figure 8. 5 grade scoring system after 4 weeks of implantation. Severity Score: 0 = finding not observed, 1 = minimal, 2 = mild, 3 = moderate, 4 = marked, 5 = severe. Distribution modifier: D = diffuse, F = focal, M = multifocal. P = non-gradable finding is present, NP = tissue/slide not present. Microscopic findings identified in control animals are common spontaneous observations that occur in toxicologic pathology studies.

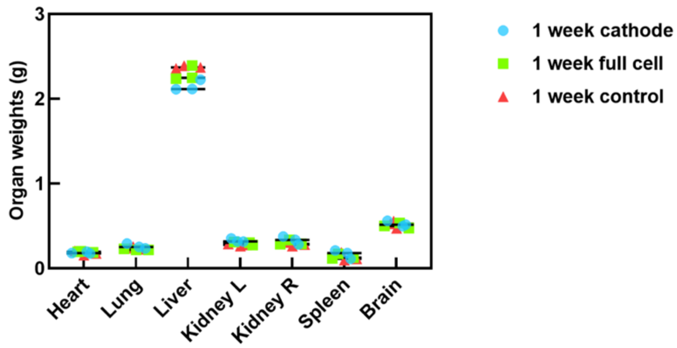

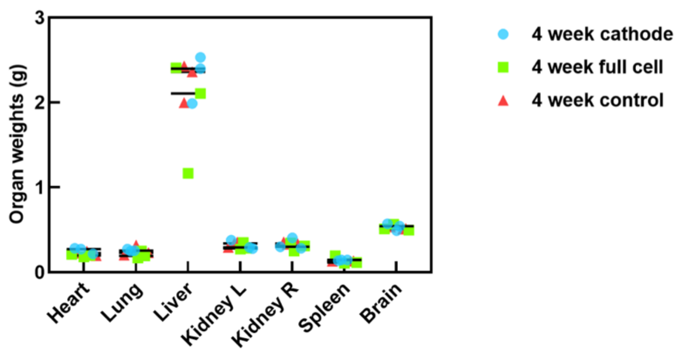

Supplementary Figure 9. Organ Weights at 1- and 4-week timepoints. Statistical analyses indicate no significant difference between cathodes, eco/bioresorbable cells, and controls at both 1- and 4-week timepoints (P = 0.9998 at 1-week and P = 0.9705 at 4-weeks). n=3 independent animals per group.

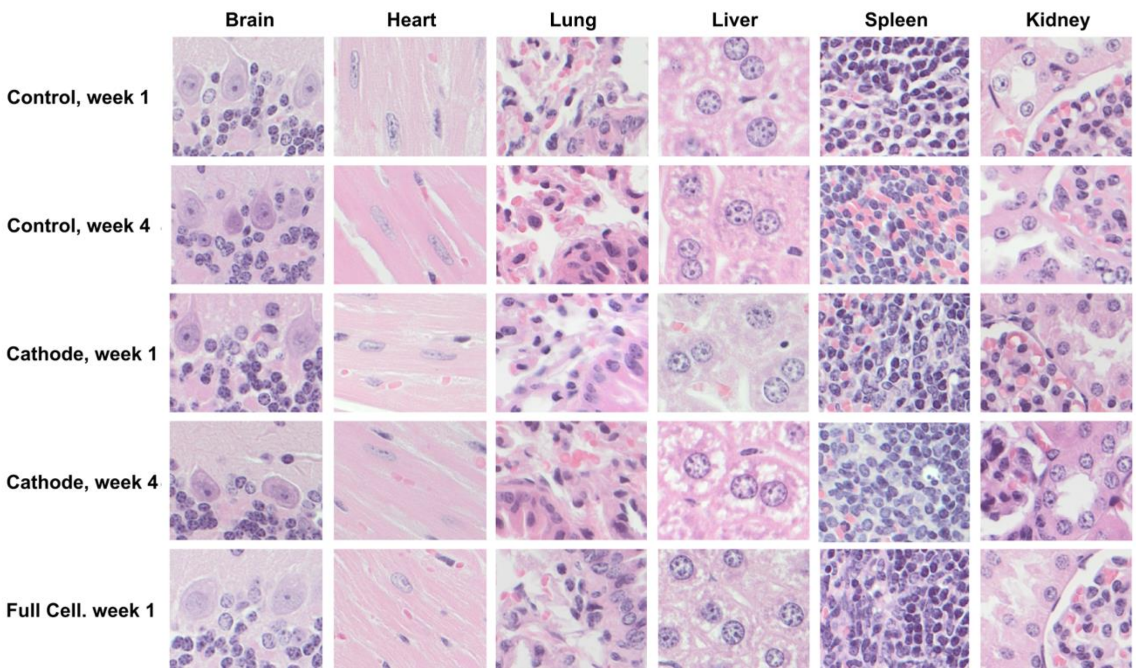

Supplementary Figure 10. No evidence of systemic toxicity was observed in sections of mouse brain, heart, lung, spleen or kidney (left to right) from any treated groups. HE, 400x.

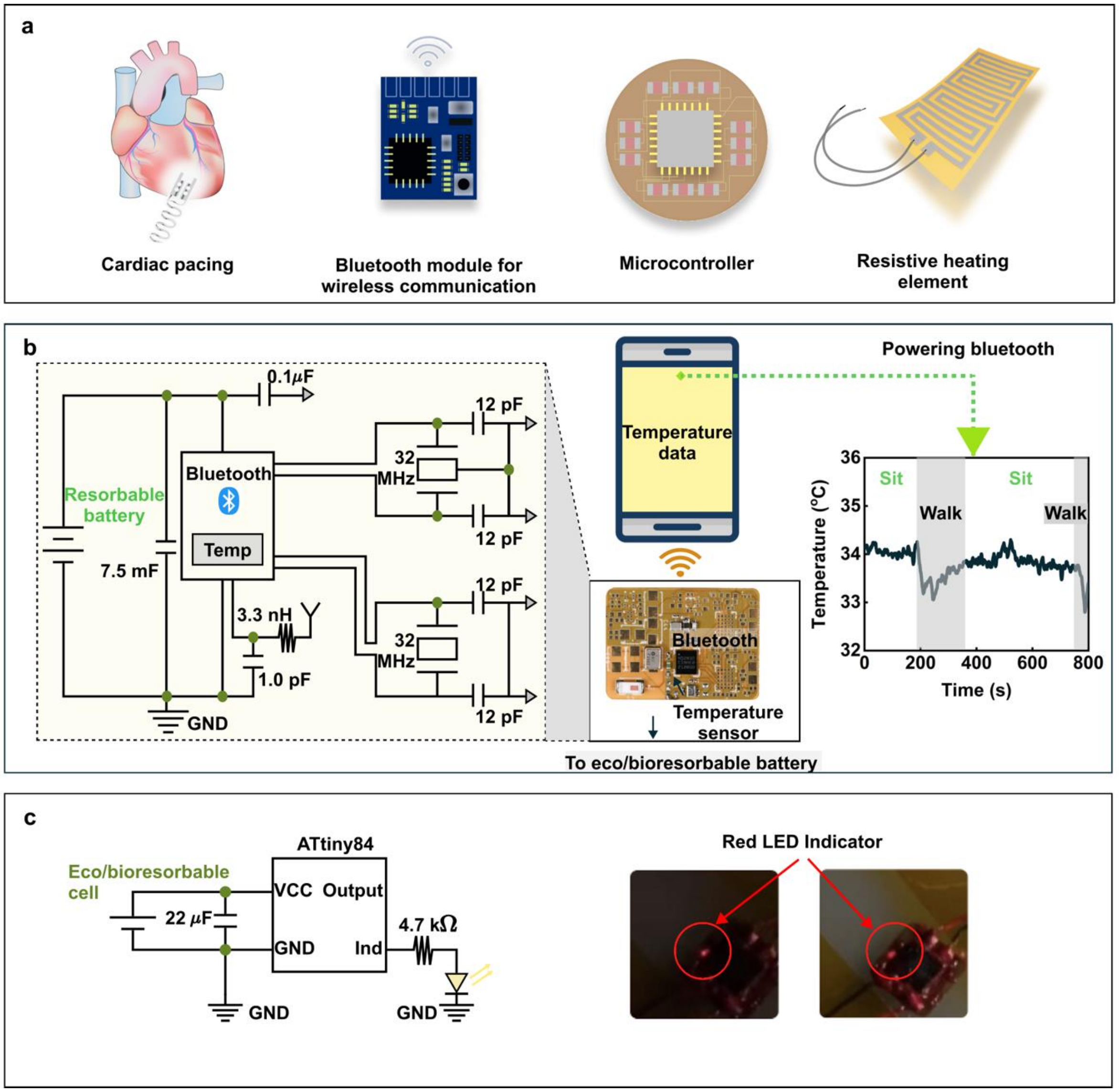

Supplementary Figure 11. Utilization of cells for thermal therapy, temperature measurements and cardiac pacing. a, Overview of applications. **b,** Demonstration of two eco/bioresorbable cells in series powering a Bluetooth Low Energy (BLE) system that performs temperature measurements and communicates relevant information to a smartphone. *(Left)* Circuit of the system. *(Center)* Photograph of the integrated temperature sensor. *(Right)* Real-time temperature measurements on the forehead of a human subject. **c,** Demonstration of a single eco/bioresorbable cell powering a microcontroller. *(Left)* Circuit of the system. *(Right)* Photograph of LED lighting up, illustrating the system successfully powers on.

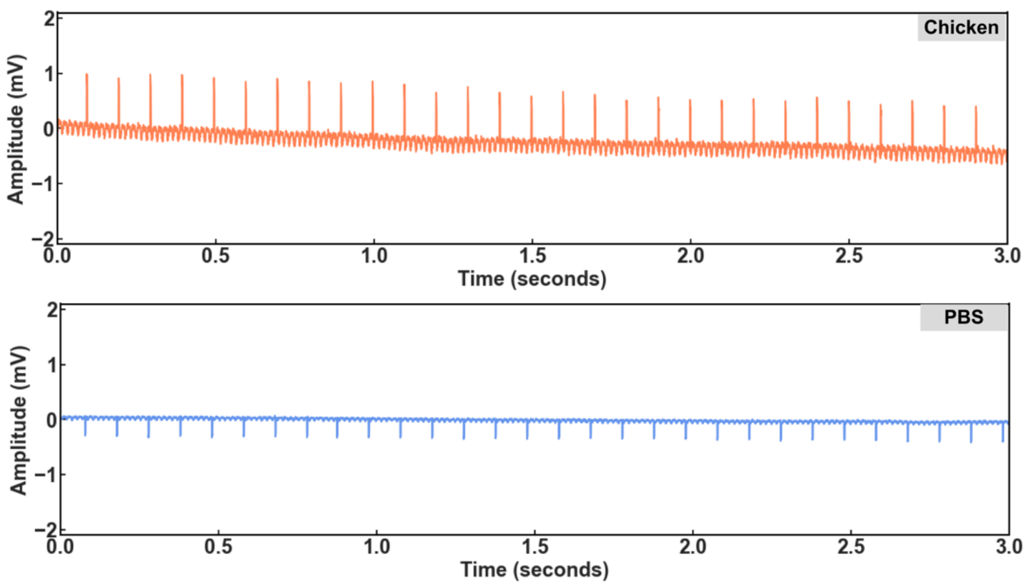

Supplementary Figure 12. Results of benchtop pacing experiments on a piece of chicken meat (top) and in PBS (bottom).

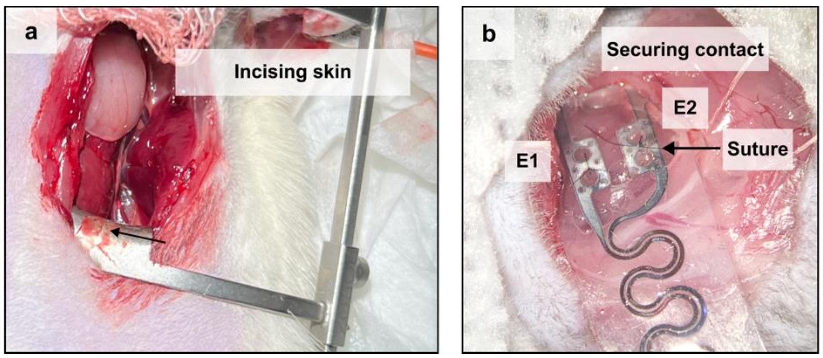

Supplementary Figure 13. Images of the surgical procedure for implanting the bioresorbable Mo electrodes. E1, E2: electrode 1 and electrode 2. The following occurs after the rodent is anesthetized and intubated. **a,** Skin on rodent is removed with clippers. Incision occurs with rodent under a microscope. Once ready, the chest retractor is inserted to open the space to the heart. **b,** Pericardial sac is cautiously moved with forceps, to enable the transient molybdenum electrodes to gently contact the left ventricle. Pacing electrodes are secured in place with sutures.

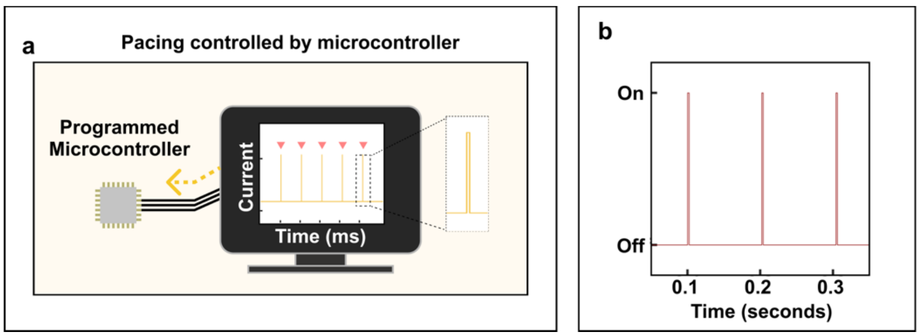

Supplementary Figure 14. Concept and circuits utilized in ex vivo demonstrations of a cell powered cardiac pacemaker on mouse hearts using a microcontroller approach. a, Microcontroller is programmed by a computer to pace at specified parameters of 2 ms on, 0.1 s off. **b,** Electrical stimulation set at 2 ms on, 0.1 s off.

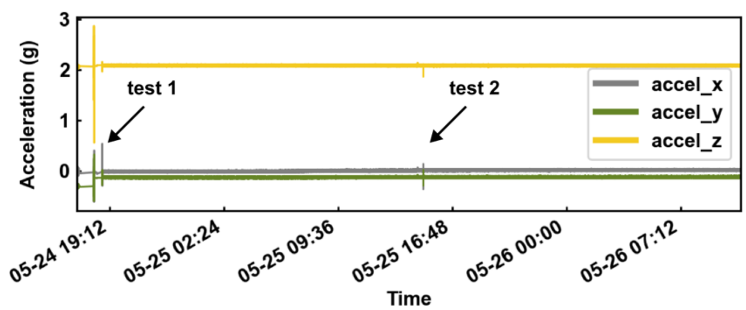

Supplementary Figure 15. 3-axis accelerometer data captured by a system on a chip (SoC) powered by the eco/bioresorbable battery implanted in ground water and soil. Two test regions reflect the intentional perturbations generated near the SoC, demonstrating the potential for capturing vibrations in real time.

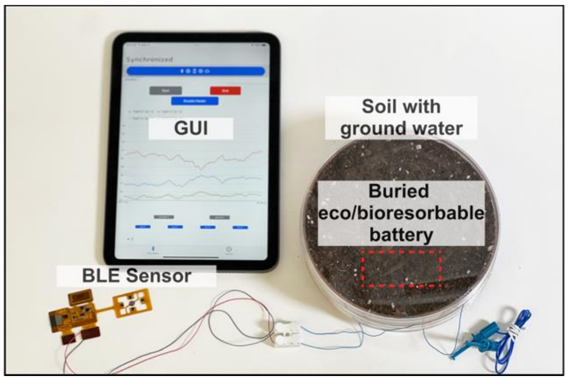

Supplementary Figure 16. Photographs of the Bluetooth Low Energy (BLE) system on a chip (SoC) connected to the eco/bioresorbable battery immersed in soil and ground water, delivering real-time measurements wirelessly to the graphical user interface (GUI).

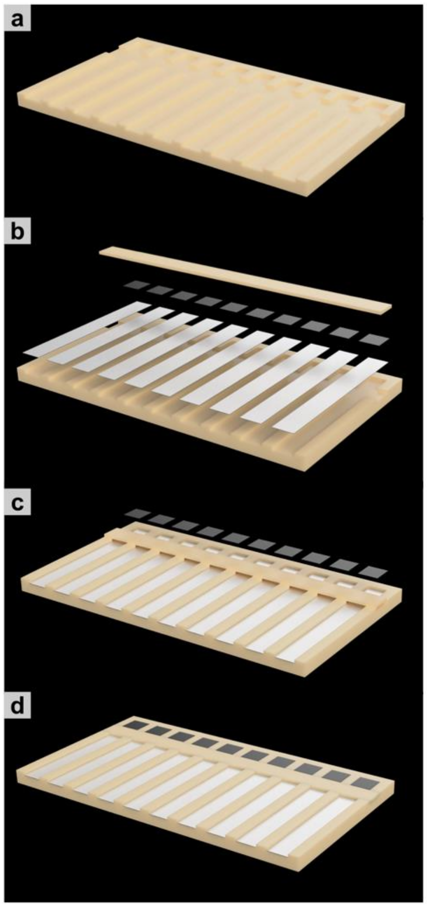

Supplementary Figure 17. Schematic illustration of the process for fabricating the cathodes (top to bottom). a, A 3D mold is designed and printed. **b,** Mo foil is placed directly within the pocket of the mold**. c,** A 3D printed spatula is placed within the pocket of the mold to secure the Mo foil in place. **d,** The iodine composite is added thereafter to deliver cathode replications.

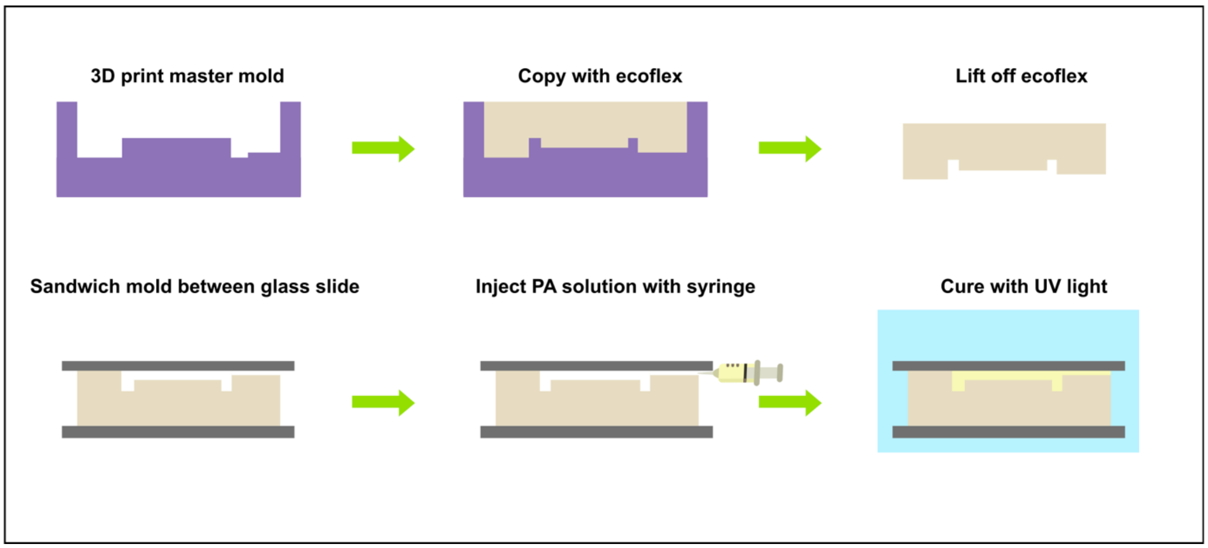

Supplementary Figure 18. Schematic illustration for the fabrication of PA films and encapsulation.

Supplementary Table 1. Comparison with reported eco/bioresorbable cells.

	Areal Capacity (mAh cm^{-2})	Voltage (V)	Areal energy (mWh cm^{-2})	Areal power (mW cm^{-2})	Volumetric energy (mWh cm^{-3})	Volumetric power (mW cm^{-3})
This work	**9.81**	**1.80**	**17.67**	**0.72**	**92.98**	**3.79**
Mg-MoO_3 [6]	1.80	1.60	2.88	0.04	7.20	0.10
Mg-FeMn [7]	0.35	0.60	0.21	0.03	3.00	0.43
Mg-Mo (1) [6]	5.60	0.60	3.36	0.02	8.40	0.04
Mg-Mo (2) [8]	2.40	0.50	1.44	0.05	5.76	0.20
Mg-Fe (1) [9] (PCL, PBS)	10.93	0.70	7.65	0.08	76.49	0.77
Mg-Fe (2) [9] (PCL, NaCl)	9.93	0.40	3.97	0.04	39.74	0.44
Mg-Fe (3) [9] (PCL, $MgCl_2$)	5.41	0.50	2.70	0.06	27.04	0.55
Mg-Fe (4) [8]	2.40	0.80	1.92	0.08	7.68	0.32
Mg-W [8]	2.40	0.70	1.68	0.07	6.72	0.28

Supplementary Table 2. Comparison with reported non-bioresorbable, implantable cells.

	Voltage (V)	Areal energy (mWh cm^{-2})	Areal power (mW cm^{-2})	Volumetric energy (mWh cm^{-3})	Volumetric power (mW cm^{-3})
This work	**1.80**	**17.67**	**0.72**	**92.98**	**3.79**
Zn-Cu [1]	0.18	38.64	0.12	89.86	0.27
Mg-Cu [1]	0.23	9.36	0.65	21.77	1.51
AZ31-Air (Au-SF) [2]	0.86	0.0013	0.02	0.08	1.01
Na(AC)-MnO_2 [3]	0.31	0.01	0.004	0.12	0.04
Na(Pyroprotein carbon)-NFP [5]	2.50	0.003	0.38	0.03	4.17
Na(NatMel)-MnO_2 [4]	0.43	0.08	0.0000043	0.76	0.000043

Supplementary Table 3. Comparison with commercial, non-degradable cells and batteries.

	Volumetric capacity (mAh cm^{-3})	Voltage (V)	Volumetric energy (mWh cm^{-3})	Specific capacity (mAh g^{-1})	Specific energy (mWh g^{-1})
This work	**51.65**	**1.80**	**92.98**	**52.49**	**94.49**
Alkaline	132.10	1.50	198.15	35.71	53.57
Zn-Ag_2O	160.21	1.55	248.33	36.67	56.83
Zinc carbon	23.32	1.50	34.99	20.00	30.00

References

(1) Nadeau, P.; El-Damak, D.; Glettig, D.; Kong, Y. L.; Mo, S.; Cleveland, C.; Booth, L.; Roxhed, N.; Langer, R.; Chandrakasan, A. P.; et al. Prolonged Energy Harvesting for Ingestible Devices. *Nat. Biomed. Eng.* **2017**, *1* (3), 22.

(2) Jia, X.; Wang, C.; Ranganathan, V.; Napier, B.; Yu, C.; Chao, Y.; Forsyth, M.; Omenetto, F. G.; MacFarlane, D. R.; Wallace, G. G. A Biodegradable Thin-Film Magnesium Primary Battery Using Silk Fibroin–Ionic Liquid Polymer Electrolyte. *ACS Energy Lett.* **2017**, *2* (4), 831–836.

(3) Kim, Y. J.; Chun, S.-E.; Whitacre, J.; Bettinger, C. J. Self-Deployable Current Sources Fabricated from Edible Materials. *J. Mater. Chem. B* **2013**, *1* (31), 3781.

(4) Kim, Y. J.; Wu, W.; Chun, S.-E.; Whitacre, J. F.; Bettinger, C. J. Biologically Derived Melanin Electrodes in Aqueous Sodium-Ion Energy Storage Devices. *Proc. Natl. Acad. Sci.* **2013**, *110* (52), 20912–20917.

(5) Lee, M. H.; Lee, J.; Jung, S.-K.; Kang, D.; Park, M. S.; Cha, G. D.; Cho, K. W.; Song, J.-H.; Moon, S.; Yun, Y. S.; et al. A Biodegradable Secondary Battery and Its Biodegradation Mechanism for Eco-Friendly Energy-Storage Systems. *Adv. Mater.* **2021**, *33* (10), 2004902.

(6) Huang, X.; Wang, D.; Yuan, Z.; Xie, W.; Wu, Y.; Li, R.; Zhao, Y.; Luo, D.; Cen, L.; Chen, B.; et al. A Fully Biodegradable Battery for Self-Powered Transient Implants. *Small* **2018**, *14* (28), 1800994.

(7) Wang, L.; Lu, C.; Yang, S.; Sun, P.; Wang, Y.; Guan, Y.; Liu, S.; Cheng, D.; Meng, H.; Wang, Q.; et al. A Fully Biodegradable and Self-Electrified Device for Neuroregenerative Medicine. *Sci. Adv.* **2020**, *6* (50).

(8) Yin, L.; Huang, X.; Xu, H.; Zhang, Y.; Lam, J.; Cheng, J.; Rogers, J. A. Materials, Designs, and Operational Characteristics for Fully Biodegradable Primary Batteries. *Adv. Mater.* **2014**, *26* (23), 3879–3884.

(9) Tsang, M.; Armutlulu, A.; Martinez, A. W.; Allen, S. A. B.; Allen, M. G. Biodegradable Magnesium/Iron Batteries with Polycaprolactone Encapsulation: A Microfabricated Power Source for Transient Implantable Devices. *Microsystems Nanoeng.* **2015**, *1* (1), 15024.